

DESIGN OF A VARIABLE GAIN INTEGRATOR WITH RESET

M.F. Heertjes¹, K.G.J. Gruntjens, S.J.L.M. van Loon, N. Kontaras, W.P.M.H. Heemels

Abstract—This paper studies the properties of a variable gain integrator with reset, i.e. a nonlinear lag filter that is obtained by a) saturating the input, b) filtering the saturated input with a Clegg integrator, and c) add the filtered output to the unsaturated input before applying it to a PID-based controller. Depending on the amount of saturation, the corner frequency of the lag filter is reduced along with the associated phase lag. This follows from a describing function analysis in which at low frequencies a minus 20 dB/decade amplitude decay is realized with a phase lag of only 32.48 degrees. Conditions to assess global asymptotic stability of the closed-loop nonlinear control system are provided that are based on a circle criterion-like argument for the flow condition, which applies to the intervals without resets, combined with a jump condition at reset. The reset integrator design is demonstrated on a piezo-actuated motion system where its favorable phase and amplitude properties induce overshoot and settling times comparable to a single (linear) integrator, but with the disturbance rejection properties of a double integrator.

I. INTRODUCTION

In this paper, we consider trade-offs between frequency domain disturbance rejection properties and time-domain overshoot and settling behavior. In particular, the fact that adding integral action to a control system often enhances the suppression of low-frequency disturbances but deteriorates transient performance in terms of overshoot and settling behavior. Given the inherent design limitations associated with linear feedback systems, nonlinear control has been proposed by many researchers in an attempt to deal with such trade-offs, e.g. the work of Aangenent *et al.* [1]. An early example is the Clegg integrator [7], i.e. an integrator which resets its single state upon zero crossings of its input. As a result of the reset, the describing function associated with the Clegg integrator has a minus 20 dB/decade amplitude decay with 38.15 degrees phase lag instead of the 90 degrees phase lag corresponding to a simple linear integrator.

A recent advancement is the variable gain integrator by Hunnekens *et al.* [8]. The variable gain integrator is a simple integrator preceded by a saturation element. Depending on the level of the saturation input signal, the integrator gain is lowered. That is, signals exceeding the saturation band will effectively lower the integrator gain, whereas signals inside the saturation band do not. Being the result of a smaller integrator buffer, an integrator design is obtained with reduced overshoot as compared to an integrator design without a saturation element. Moreover, inside the saturation bound, the variable gain integrator induces similar disturbance rejection properties as obtained with a simple integrator otherwise. In practice, however, this often means

that settling properties inside the saturation bound are equally limited by the phase delay induced by the simple integrator.

As a solution to this problem, in this paper a variable gain integrator with reset will be studied. For a piezo-actuated motion system, it will be demonstrated that less overshoot is obtained as compared to the Clegg integrator but equal to the variable gain integrator without reset. Contrarily, the settling behavior of the variable gain integrator with reset is equally fast as the settling behavior induced by the Clegg integrator, but much faster than the variable gain integrator without reset. The variable gain integrator with reset thus combines the favorable properties of the variable gain integrator without reset, i.e. reduced overshoot, with the small settling times of the Clegg integrator. From describing function analysis, this may relate to the minus 20 dB per decade amplitude decay that corresponds to only 32.48 degrees phase lag, i.e. a phase reduction of about 6 degrees with respect to the Clegg integrator.

Stability of the variable gain integrator with reset will be shown by combining a circle criterion-like argument used to prove stability of the variable gain integrator along the resets. Essentially, stability of the reset system boils down to satisfying two conditions: a) a flow condition in the intervals between resets, and b) a jump condition at the resets, see also Beker *et al.* [4], Zaccarian *et al.* [9], and Carrasco *et al.* [6]. For the base-nonlinear system, i.e. the variable gain integrator without reset in closed loop, stability is guaranteed by the application of the positive real lemma along with a LaSalle argument to deal with the simple pole. This renders the base-nonlinear system globally asymptotically stable, thus satisfying the flow condition. For the closed-loop nonlinear system with reset, we seek a positive-definite matrix $P \succ 0$ that satisfies both the flow and the jump condition. This will be done by solving a set of linear matrix inequalities (LMIs).

Summarizing, the main contributions of this paper are as follows. First, the variable gain integrator of Hunnekens *et al.* [8] is extended with a reset condition that is introduced to maintain the disturbance properties associated with a double integrator, but that significantly improves the settling behavior inside the saturation length toward the behavior of a single integrator. Second, a describing function analysis is presented to demonstrate the nonlinear lag-filter properties of the design. Third, sufficient Lyapunov-based stability conditions are provided that can be verified using standard LMI-solvers. Fourth, the potential of the proposed nonlinear controller is shown by means of experimental results on an industrially-relevant piezo-actuated motion system.

The remainder of this paper is organized as follows. In Section II, the variable gain integrator with reset will be presented, whereas its properties will be studied using de-

¹ All authors are with Eindhoven University of Technology, 5600 MB Eindhoven, The Netherlands. Marcel F. Heertjes is also with ASML, Veldhoven, The Netherlands. Please direct all correspondence to this author. m.f.heertjes@tue.nl

scribing function analysis. In Section III the problem setting will be described including the motivation for the variable gain integrator with reset on the basis of experimental results obtained from a piezo-actuated motion system. In Section IV the base-nonlinear system, i.e. the variable gain integrator without reset in closed loop with a PID-based controller and double-integrator-based motion system will be given along with a short review of its closed-loop stability properties. In Section V, new stability conditions will be posed for the variable gain integrator with reset in closed loop. Section VI will summarize the main conclusions.

The following notational conventions will be used. Let \mathbb{R} denote the set of real numbers and \mathbb{R}^n denote the n -fold Cartesian product $\mathbb{R} \times \dots \times \mathbb{R}$ with standard Euclidean norm denoted by $\|\cdot\|$. For a matrix $S \in \mathbb{R}^{n \times m}$, we denote by $\text{im}S := \{Sv \mid v \in \mathbb{R}^m\}$ the image of S , and by $\text{ker}S := \{x \in \mathbb{R}^m \mid Sx = 0\}$ its kernel. We call a matrix $P \in \mathbb{R}^{n \times n}$ positive definite and write $P \succ 0$, if P is symmetric (i.e., $P = P^\top$) and $x^\top Px > 0$ for all $x \neq 0$. Similarly, we call $P \prec 0$ negative definite when $-P$ is positive definite.

II. VARIABLE GAIN INTEGRATOR WITH RESET

Consider the variable gain integrator with reset as shown in Fig. 1. It consists of a variable gain part, see Hunnekens *et*

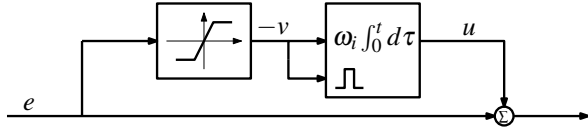


Fig. 1. Graphical representation of the reset integrator design.

al. [8], i.e. a saturation function between the input signal $e(t)$ and the internal signal $v(t) = -\phi(e(t))$, a Clegg integrator [7] that resets its integrator state upon zero crossings of $v(t)$, and a direct path that gives the overall output signal $u(t) + e(t)$. The saturation function $\phi(e)$ is defined as

$$\phi(e) = \begin{cases} e, & \text{if } |e| \leq \delta \\ \delta \text{sign}(e), & \text{otherwise,} \end{cases} \quad (1)$$

with saturation length $\delta \geq 0$, whereas the Clegg integrator in state-space description is given by

$$\begin{cases} \dot{x}_I(t) = \omega_i v(t), & \text{if } v(t) \neq 0, \\ u(t) = x_I(t), & \\ x_I(t^+) = 0, & \text{otherwise,} \end{cases} \quad (2)$$

with $x_I(t)$ denoting the integrator state, ω_i the integrator frequency, and t^+ denoting a time instance where $v(t)$ crosses zero. To better understand the properties associated with the reset integrator design from Fig. 1, a describing function analysis will be carried out that allows for frequency domain evaluation through Bode diagrams.

A. Describing Function Analysis

In this section, we provide a describing function analysis of the variable gain integrator with reset. To do so, let e be a sinusoidal input signal given by

$$e(\tau) = \hat{e} \sin(\tau), \quad (3)$$

with amplitude \hat{e} and $\tau = \omega t$. Consider the case where the input signal $e(t)$ is saturated, i.e. $0 < \delta < \hat{e}$. Using (1), the saturated signal $v(\tau) = -\phi(e(\tau))$ for $0 \leq \tau < \pi$ reads:

$$v(\tau) = \begin{cases} \hat{e} \sin(\tau), & \text{if } 0 \leq \tau < \gamma \\ \delta, & \text{if } \gamma \leq \tau < \pi - \gamma \\ \hat{e} \sin(\tau), & \text{if } \pi - \gamma \leq \tau < \pi, \end{cases} \quad (4)$$

where it holds that $\gamma = \arcsin(\delta/\hat{e})$, see also the upper part of Fig. 2. By forward integration using (2), it therefore follows for the signal $u(\tau)$:

$$u(\tau) = \begin{cases} -\frac{\omega_i}{\omega} \hat{e} \cos(\tau) + c_1, & \text{if } 0 \leq \tau < \gamma \\ \frac{\omega_i}{\omega} \delta \tau + c_2, & \text{if } \gamma \leq \tau < \pi - \gamma \\ -\frac{\omega_i}{\omega} \hat{e} \cos(\tau) + c_3, & \text{if } \pi - \gamma \leq \tau < \pi, \end{cases} \quad (5)$$

with integration constants:

$$\begin{aligned} c_1 &= \frac{\omega_i}{\omega} \hat{e} \\ c_2 &= \frac{\omega_i}{\omega} \left(\hat{e} \left(1 - \gamma \sqrt{1 - \sin^2(\gamma)} \right) - \delta \gamma \right) \\ c_3 &= \frac{\omega_i}{\omega} \left(\hat{e} \left(1 - 2\gamma \sqrt{1 - \sin^2(\gamma)} \right) - 2\delta \gamma \right) + \frac{\omega_i}{\omega} \delta \pi, \end{aligned} \quad (6)$$

see also the lower part of Fig. 2. The describing function

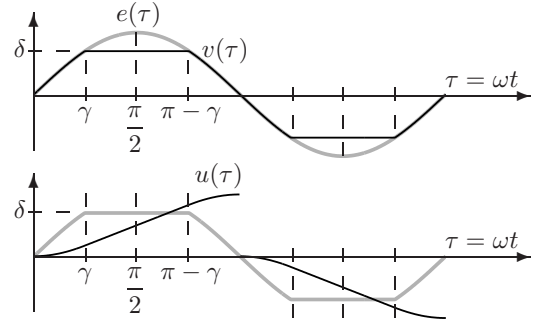


Fig. 2. Graphical representation of the variable gain (upper) part: from a sinusoidal input $e(\tau) = \hat{e} \sin(\tau)$ to saturation output $v(\tau)$, and the reset (lower) part from $v(\tau)$ to $u(\tau)$.

$N(\hat{e}, \omega)$ between harmonic input e and resulting output $u + e$ is given by:

$$N(\hat{e}, \omega) = 1 + \frac{b_1 + ja_1}{\hat{e}}, \quad (7)$$

with

$$\begin{aligned} a_1 &= \frac{2}{\pi} \int_0^\pi u(\tau) \cos(\tau) d\tau \\ b_1 &= \frac{2}{\pi} \int_0^\pi u(\tau) \sin(\tau) d\tau. \end{aligned} \quad (8)$$

Substitution of (5) and (6) in (8) gives (after some algebra):

$$\begin{aligned} a_1 &= \frac{2\omega_i}{\pi\omega} \left(-\delta \sqrt{1 - \left(\frac{\delta}{\hat{e}} \right)^2} - \hat{e} \gamma \right) \\ b_1 &= \frac{2\omega_i}{\pi\omega} \left(2\hat{e} \left(1 - \sqrt{1 - \left(\frac{\delta}{\hat{e}} \right)^2} \right) + \delta \pi - 2\delta \gamma \right). \end{aligned} \quad (9)$$

For the case where the input signal $e(t)$ is not saturated, i.e. $0 < \hat{e} \leq \delta$, it follows that:

$$\begin{aligned} a_1 &= \frac{2\omega_i}{\pi\omega} \left(-\frac{\hat{e}\pi}{2} \right) = -\frac{\omega_i\hat{e}}{\omega} \\ b_1 &= \frac{2\omega_j}{\pi\omega} (2\hat{e}) = \frac{4\omega_j\hat{e}}{\pi\omega}. \end{aligned} \quad (10)$$

Note that when $\hat{e} \rightarrow \delta$, (9) tends to (10). Moreover for the trivial case where $\delta = 0$, i.e. neither saturation nor integration with reset takes place, it follows that $a_1 = b_1 = 0$.

By substitution of either (9) or (10) in (7), depending on the parameter values for δ and \hat{e} , Fig. 3 shows the Bode diagrams. For the curve where $\delta/\hat{e} = 1$, a lag filter results.

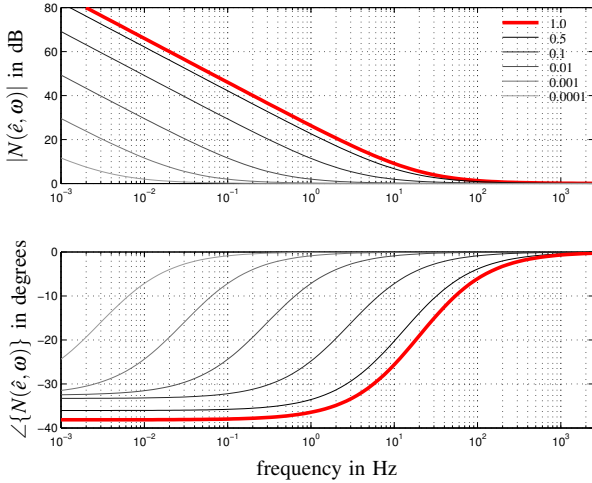


Fig. 3. Bode diagrams of different describing functions of the reset integrator design from e to $e+u$ for $\delta/\hat{e} \in \{0.0001, 0.001, 0.01, 0.1, 0.5, 1\}$.

Namely, substitution of (10) in (7) gives

$$N(\hat{e}, \omega) \rightarrow 1 + \frac{\omega_i}{j\omega} \left(1 + \frac{4}{\pi} j \right), \text{ if } 0 < \hat{e} \leq \delta. \quad (11)$$

At high frequencies the frequency response tends to unity whereas at low frequencies a Clegg integrator is obtained, i.e. a simple integrator multiplied with the complex number $\omega_i(1 + 4j/\pi) \approx 1.619\omega_i \exp(j51.85)$. As a result, Fig. 3 shows a 20dB/decade amplitude decay with a phase lag of only $\approx 90 - 51.85 = 38.15$ degrees; increasing the ratio δ/\hat{e} does not change these properties. Decreasing the ratio δ/\hat{e} , i.e. saturating the input signal $e(t)$, shows two effects: a) the corner frequency of the lag filter decreases as the integrator part decreases, and b) the phase lag of the integrator part further decreases. The latter follows from the fact that:

$$\arcsin\left(\frac{\delta}{\hat{e}}\right) \rightarrow \frac{\delta}{\hat{e}} \text{ and } \sqrt{1 - \left(\frac{\delta}{\hat{e}}\right)^2} \rightarrow 1 \text{ for } \hat{e} \gg \delta, \quad (12)$$

which substituted in (9) and using (7) gives

$$N(\hat{e}, \omega) \rightarrow 1 + \frac{\omega_i\delta}{\pi j\omega\hat{e}} \left(2\pi j - \frac{4\delta}{\hat{e}} j + 4 \right) \text{ for } \hat{e} \gg \delta, \quad (13)$$

and with $\delta > 0$. At low-frequencies, this gives rise to a phase lag limit of 32.48 degrees as can be seen in Fig. 3.

III. PIEZO-ACTUATED MOTION SYSTEM

To demonstrate the effectiveness of the variable gain integrator with reset in dealing with linear design limitations, consider the control of a piezo-actuated motion system that is used in wafer scanners. During the process of wafer scanning light from an (extreme) ultra-violet source travels through an optical path that includes a reticle containing a blueprint of the integrated circuits to be processed and a lens system. The lens system consists of several lens elements that are individually controlled during the scanning process. This poses the following problem.

A. PROBLEM SETTING

Given the limited stroke of the piezo actuators, a calibration, or so-called shuffle, needs to be performed whenever stroke limitations are encountered. Such a shuffle may occur more than once during full wafer exposure. It is clear that the duration of the shuffle should be kept small. This is because during shuffle, the scanning process is interrupted and therefore machine throughput, i.e. the amount of wafers that can be processed per unit of time, is compromised. Furthermore, during shuffle mode the piezo-actuated system operates in an open-loop state such that after the shuffle, i.e. after closing the loop, the motion system, which then operates in scanning mode, suffers from an initial value problem. This problem even becomes more pronounced in view of the disturbance rejection properties required during scanning mode for which a PI²D controller, i.e. a controller with two integrators, is preferred over PID control with one integrator only.

B. MEASUREMENT RESULTS

Given the above problem setting, the effect of the variable gain integrator with reset from Fig. 1 is demonstrated in Fig. 4. Through time-series measurement¹ on a state-

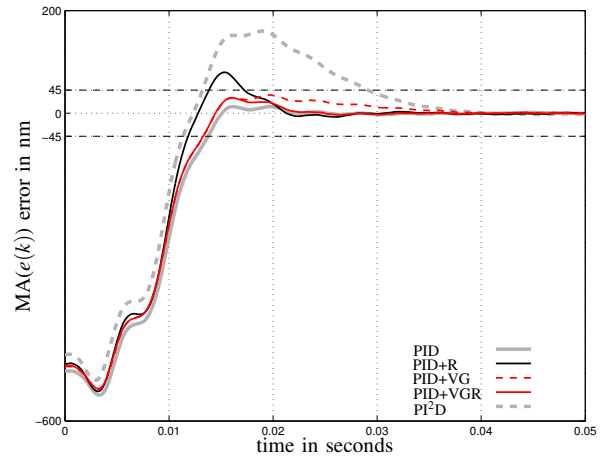


Fig. 4. Moving average (MA) filtered error responses of measurement data from a piezo-actuated lens system under different controller configurations: a) PID, b) PID and a Clegg integrator (PID+R), c) PID and a variable gain integrator without reset (PID+VG), d) PID and a variable gain integrator with reset (PID+VGR), and e) PI²D.

of-the-art piezo-actuated lens system of a wafer scanner, the figure shows the results in scanning mode after five identical shuffles with different controller configurations: a) PID control, b) PID control and a Clegg integrator, c) PID control and a variable gain integrator without reset, d) PID control and the variable gain integrator with reset, and e) PI²D control. The results in terms of moving average (MA) filtered error signals appear to be very illustrative, though the actual time instances of reset at $e(t) = 0$ are not immediately detectable from these (filtered) responses. Having desired disturbance rejection properties in scanning mode, PI²D control induces significantly more overshoot and a larger settling time compared to PID control. Contrarily, PID control in combination with the variable gain integrator shows a significant reduction of the overshoot according to what is claimed in Hunnekens *et al.* [8], while preserving the desired disturbance rejection properties in scanning mode. In fact, inside the saturation band of 45 nm the controller properties become identical to PI²D control, which comes with the disadvantage of too long settling times (dashed red curve). The variable gain integrator with reset (red curve) perfectly combines the advantage of small overshoot from the variable gain integrator without reset with the small settling times associated with a Clegg integrator. The latter follows from PID control in combination with a Clegg integrator (black curve) that induces less favorable overshoot in comparison with the variable gain integrator, but with desirable settling behavior related to the reduced phase lag.

Having a clear industrial motivation, at this point in the analysis we want to study (in depth) the stability properties of the variable gain integrator with reset when being used in closed loop with an additional controller and motion system. To do so, we will first study the base-nonlinear system, i.e. the variable gain integrator without reset.

IV. BASE-NONLINEAR SYSTEM

Consider the motion control structure without any reset such as depicted in Fig. 5, with reference r used to dictate

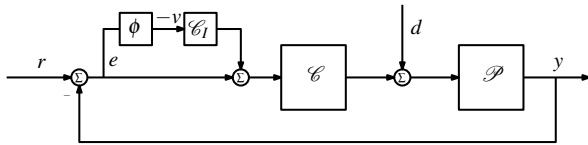


Fig. 5. Block diagram of the base-nonlinear system, i.e. the motion control structure without the reset part.

point-to-point motion and the error signal $e = r - y$. Herein y is the output of the linear-time invariant (LTI) motion system \mathcal{P} , which is subject to disturbances d , and which is controlled in feedback by the LTI controller \mathcal{C} . The variable gain integrator design in Fig. 5 will be referred to as the base-nonlinear system, where ϕ is defined by (1) and \mathcal{C}_I is given in frequency domain by

$$\mathcal{C}_I(s) = \frac{\omega_i}{s} \quad (14)$$

¹Numerical simulations based on second-order parametric models show very similar results. Furthermore, various experiments under different initial conditions demonstrated comparable behavior.

with $s \in \mathbb{C}$ the Laplace variable. The transfer function between e and v (with $r = d = 0$) is then given by

$$\frac{e(s)}{v(s)} = G(s) = \frac{\omega_i}{s} \underbrace{\frac{\mathcal{C}(s)\mathcal{P}(s)}{1 + \mathcal{C}(s)\mathcal{P}(s)}}_{\mathcal{S}_c(s)}, \quad (15)$$

with $\mathcal{S}_c(s)$ the complementary sensitivity function and with $G(s)$ having a simple pole at $s = 0$.

A representative motion system \mathcal{P} is shown in Bode representation in Fig. 6. Both a second-order parametric model

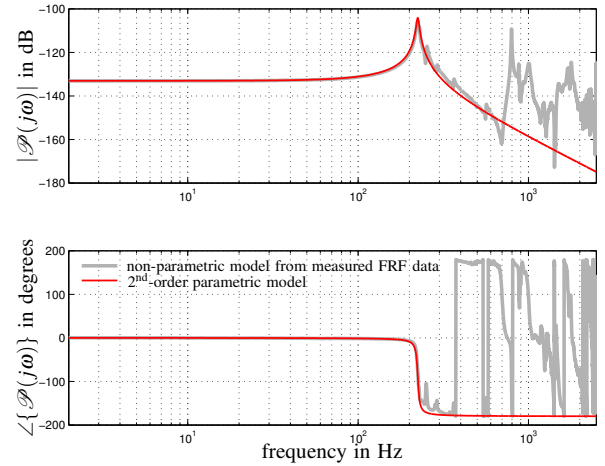


Fig. 6. Bode diagram of a non-parametric model obtained from measured FRF data coming from a piezo-actuated motion system and a simplified second-order parametric model fit.

as well as a non-parametric model obtained from measured frequency response function (FRF) data and coming from the previously introduced piezo-actuated motion system are shown. Both models are used to illustrate the main ideas of this paper.

A. STATE-SPACE MODEL

In the time domain the closed-loop dynamics of the base-nonlinear system can be represented by the state-space model

$$\begin{aligned} \dot{x}(t) &= Ax(t) + Bv(t) + B_r r(t) + B_d d(t) \\ e(t) &= Cx(t) + D_r r(t) + D_d d(t) \\ v(t) &= -\phi(e(t)), \end{aligned} \quad (16)$$

with state vector $x(t) = [x_I(t) \ \tilde{x}(t)^T]^T \in \mathbb{R}^n$ at time $t \in \mathbb{R}_{\geq 0}$, in which $x_I \in \mathbb{R}$ denotes the state of the linear integrator \mathcal{C}_I and $\tilde{x} \in \mathbb{R}^{\tilde{n}}$ consists of both the states of the plant \mathcal{P} as well as the states of the LTI controller \mathcal{C} . Note that $G(s)$ as in (15) satisfies $G(s) := C(sI - A)^{-1}B$, where we assume that (A, B, C) corresponds to a minimal realization.

B. STABILITY

Consider the base-nonlinear system for constant references $r(t) = r_c$ and constant disturbances $d(t) = d_c$, $t \in \mathbb{R}_{\geq 0}$. In this case, there is a unique equilibrium with $e = 0$ corresponding to $x^* = [x_I^* \ \tilde{x}^{*T}]^T$ (clearly, x^* depends on both r_c and d_c). The following result (see also Hunnekens *et al.* [8]) poses sufficient conditions under which global asymptotic stability (GAS) of the equilibrium x^* can be guaranteed.

Proposition 1: Consider system (16) with constant reference r_c and constant disturbance d_c . If the following conditions are satisfied:

$$\begin{aligned} \text{i)} \quad & \mathcal{L}_c(0) \geq 0 \\ \text{ii)} \quad & \mathcal{L}_c(j\omega) \text{ is Hurwitz} \\ \text{iii)} \quad & \Re\{G(j\omega)\} \geq -1, \forall \omega \in \mathbb{R}, \end{aligned} \quad (17)$$

then the equilibrium point $x = x^*$ of system (16) satisfying $e = 0$ is GAS.

Proof: [Sketch of proof]

For the detailed proof, the reader is referred to Hunnekens *et al.* [8]. Here it suffices to state that a circle criterion argument is adopted, see also Arcak *et al.* [2]. Key in this argument is the application of the positive real lemma (rather than the strictly positive real lemma) together with a LaSalle argument used to conclude GAS of the equilibrium point $x = x^*$; the strictly positive real lemma cannot be used due to the simple pole $j\omega = 0$ of $G(j\omega)$ in (15). ■

Remark 1: For the piezo-actuated motion system from Fig. 6, the conditions in (17) can be checked as follows: i) $\mathcal{L}_c(0) \geq 0$ is satisfied as (15) equals one (by design) for $\omega = 0$, ii) $\mathcal{L}_c(j\omega)$ being Hurwitz follows for any minimal realization of a stabilizing linear control design, and iii) $\Re\{G(j\omega)\} \geq -1, \forall \omega \in \mathbb{R}$ is graphically shown to be satisfied in Fig. 7, for the non-parametric model based on

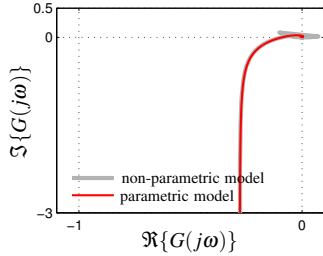


Fig. 7. Nyquist diagram showing that $\Re\{G(j\omega)\} \geq -1$ is satisfied either with the non-parametric or the parametric model from Fig. 6.

measured FRF data, and the parametric second-order model.

Furthermore, it is important to realize that satisfying (17) implies the existence of $P \succ 0$ such that $V(z) = z^T P z > 0$ for $z \neq 0$, and $\dot{V}(z) \leq 0$ with $z = x - x^*$ a coordinate transformation used to shift the equilibrium $x = x^*$ to the origin; note that an equilibrium point of (16) implies $e = 0$ due to the integrator in $\mathcal{C}(s)$ and the fact that $\phi(e) = 0$ only holds true for $e = 0$. Given this transformation, (16) can be written (for constant r and constant d) as

$$\begin{aligned} \dot{z}(t) &= Az(t) + Bv(t) \\ e(t) &= Cz(t) \\ v(t) &= -\phi(e(t)). \end{aligned} \quad (18)$$

In particular, the Lyapunov function V essentially satisfies

$$\dot{V}(z) = z^T (A^T P + PA)z + v^T B^T P z + z^T P B v \leq 0, \quad (19)$$

or, alternatively:

$$\begin{bmatrix} z \\ v \end{bmatrix}^T \begin{bmatrix} A^T P + PA & PB \\ B^T P & 0 \end{bmatrix} \begin{bmatrix} z \\ v \end{bmatrix} \leq 0, \quad (20)$$

when for all v and e (or z) satisfying the sector condition $v^2 + ve \leq 0$. In fact, using the S-procedure, see e.g. Boyd [5], leads to the condition that there exists $\tau \geq 0$ such that

$$\begin{bmatrix} A^T P + PA & PB - \frac{\tau}{2} C^T \\ B^T P - \frac{\tau}{2} C & -\tau \end{bmatrix} \preceq 0. \quad (21)$$

Having the conditions in (17) to check for GAS of the equilibrium of the base-nonlinear system (16) and having the means to find an explicit $P \succ 0$ by solving the LMIs in (21), we want to extend the closed-loop stability result to the case when the integrator \mathcal{C}_I in Fig. 5 is allowed to reset.

V. CLOSED-LOOP STABILITY UNDER RESET

Consider the closed-loop dynamics as depicted in Fig. 8. The variable gain integrator with reset element from Fig. 1

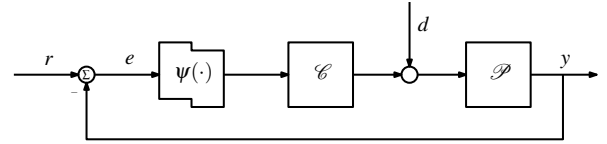


Fig. 8. Block diagram of a motion control structure with variable gain integrator with reset element $\psi(\cdot)$.

is denoted by $\psi = \psi(e)$.

A. STATE-SPACE MODEL WITH RESET

In state-space representation, the dynamics underlying Fig. 8 can be represented by

$$\begin{cases} \dot{x}(t) = Ax(t) + Bv(t) + B_r r(t) + B_d d(t) \\ e(t) = Cx(t) + D_r r(t) + D_d d(t) \\ v(t) = -\phi(e(t)), \end{cases} \quad \text{if } x(t) \notin \mathcal{M} \quad (22a)$$

$$x(t^+) = A_R x(t), \quad \text{if } x(t) \in \mathcal{M} \quad (22b)$$

with

$$A_R = \begin{bmatrix} 0 & O_{1 \times \bar{n}} \\ O_{\bar{n} \times 1} & I_{\bar{n} \times \bar{n}} \end{bmatrix}, \quad (22c)$$

in which I denotes the identity matrix and O a matrix containing zeros, and the set \mathcal{M} is given by

$$\mathcal{M} := \{x \in \mathbb{R}^n \mid Cx = 0, (I - A_R)x \neq 0\}. \quad (22d)$$

Note that, in (22d) the condition $(I - A_R)x \neq 0$ was added to avoid multiple jumps at one time instant. As a standing assumption, we assume that the overall system (22) produces complete and non-Zeno solutions in the terminology of [10, Definition 2.5], for all relevant initial conditions, references and disturbances, i.e. solutions are defined for all $t \in \mathbb{R}_{\geq 0}$. In the current control configuration as depicted in Fig. 8, the integrator state $x_I \in \mathbb{R}$ is reset to zero when $v(t) = 0$, for all $t \in \mathbb{R}_{\geq 0}$. Hence, different from solutions to (16), the solutions to (22) are (partly) discontinuous, which is implied by the additional reset condition (22b).

B. STABILITY WITH RESET

Let x^* be defined as the unique equilibrium point of system (22) satisfying

$$0 = Ax^* + B_r r_c + B_d d_c \quad (23a)$$

$$0 = Cx^* + D_r r_c + D_d d_c, \quad (23b)$$

and, due to (23b) also $v = 0$ (due to $e = 0$), which implies

$$x^* = A_R x^*. \quad (23c)$$

The following theorem poses sufficient conditions under which GAS of the equilibrium $x = x^*$ can be guaranteed for the system in (22). In order to do so, the matrix $\Theta \in \mathbb{R}^{n \times (n-1)}$ is defined as $\text{im}(\Theta) = \ker(C)$.

Theorem 1: Consider the system in (22). If there exist a positive definite matrix $P \in \mathbb{R}^{n \times n}$ and a constant $\tau \in \mathbb{R}_{\geq 0}$, satisfying

$$\begin{bmatrix} A^T P + PA & PB - \frac{\tau}{2} C^T \\ B^T P - \frac{\tau}{2} C & -\tau \end{bmatrix} \preceq 0 \quad (24)$$

$$\Theta^T (A_R^T P A_R - P) \Theta \preceq 0, \quad (25)$$

then the corresponding equilibrium point $x = x^*$ of system (22) is globally asymptotically stable for any constant reference r_c and constant disturbance d_c .

Proof: [Sketch of proof]

The first step is to employ a coordinate transformation $\tilde{z} = x - x^*$ on (22) giving:

$$\begin{cases} \dot{\tilde{z}} = A\tilde{z} + Bv \\ e = C\tilde{z} \\ v = -\phi(e(t)), \end{cases} \quad \text{if } \tilde{z} \notin \tilde{\mathcal{M}}, \quad (26a)$$

$$\tilde{z}^+ = A_R \tilde{z}, \quad \text{if } \tilde{z} \in \tilde{\mathcal{M}} \quad (26b)$$

with $\tilde{\mathcal{M}} := \{\tilde{z} \in \mathbb{R}^n \mid C\tilde{z} = 0, (I - A_R)\tilde{z} \neq 0\}$.

In the second step, we will show that $V(\tilde{z}) = \tilde{z}^T P \tilde{z}$, with $P = P^T \succ 0$, satisfying (24) and (25), is a Lyapunov function for the transformed (perturbed) dynamics in (26). In fact, during flow, feasibility of (24) guarantees that

$$\dot{V}(\tilde{z}) \leq 0, \quad \text{for } \tilde{z} \notin \tilde{\mathcal{M}}, \quad (27)$$

along the solutions of (26), and feasibility of (25) guarantees that during resets

$$V(A_R \tilde{z}) - V(\tilde{z}) \leq 0, \quad \text{for } \tilde{z} \in \tilde{\mathcal{M}}, \quad (28)$$

i.e. the Lyapunov function does not increase during resets.

Note that (27) together with (28) implies Lyapunov stability of $\tilde{z} = 0$, however, not yet GAS. To establish GAS of $\tilde{z} = 0$, a LaSalle argument is used for hybrid systems, see [10], in which we also exploited the observations in [8], which were already remarked in the sketch of proof of Proposition 1. As a consequence, it follows that $x = x^*$ is a GAS equilibrium point of (22), which completes the proof. ■

Remark 2: In practice, a preferable stability check would be a graphical check similar to the circle criterion evaluation in Fig. 7. The reason is that solving the LMIs in (24) and (25) requires a parametric model which for real applications

is time-consuming to obtain and often not accurate enough. The use of non-parametric models based on measured FRF data, which are both easily obtained and accurate, is therefore highly preferred in posing the stability conditions.

Remark 3: Feasibility of the LMIs in (24) and (25) turned out to be difficult to obtain in the case of the Clegg integrator. In fact, feasibility has only been obtained when replacing the specific Clegg integrator by the more general first-order reset element (FORE) [11], i.e. using a weak integrator instead of a simple integrator. Physically, this can be understood from the reduced phase lag that has a stabilizing effect. As an additional advantage, using a FORE (and excluding the specific case of the Clegg integrator) renders the need for the LaSalle argument in (17) superfluous, i.e. we can reside to the strictly positive real lemma to conclude GAS of the equilibrium point $x = x^*$.

VI. CONCLUSIONS

In this paper, a variable gain integrator design with reset is discussed. The design has disturbance rejection properties associated with a double integrator but with the overshoot and settling properties related to a single integrator. For a piezo-actuated motion system, these properties appear very useful in dealing with the initial value problem resulting from a shuffle and occurring prior to scanning. By reducing overshoot and settling times, wafer exposure is less delayed, i.e. enhanced wafer throughput, which has been demonstrated by experimental results. Furthermore, Lyapunov-based stability conditions are presented. Solving P with LMI-solvers, however, requires parametric models which are time-consuming to obtain and often not accurate enough. Future work will therefore focus on non-parametric models, i.e. measured FRF data.

REFERENCES

- [1] W.H.T.M. Aangenent, G. Witvoet, W.P.M.H. Heemels, M.J.G. Van De Molengraft, and M. Steinbuch. (2010) Performance analysis of reset control systems, *Int. J. of Robust and Nonlinear Control*, 20(11), pp.1213-1233.
- [2] M. Arcak, M. Larsen, and P. Kokotovic. (2003) Circle and Popov criteria as tools for nonlinear feedback design. *Automatica*, 39(4), pp. 643650.
- [3] A. Baños, and A. Barreiro. (2012) *Reset control systems*, Springer, London.
- [4] O. Beker, C.V. Hollot, Y. Chait, and H. Han. (2004) Fundamental properties of reset control systems, *Automatica*, 40, pp. 905-915.
- [5] S.P. Boyd, L. El Ghaoui, E. Feron, and V. Balakrishnan. (1994) *Linear matrix inequalities in system and control theory*, SIAM Studies in Applied Mathematics, Vol. 15, Philadelphia, Pennsylvania.
- [6] J. Carrasco, A. Baños, and A. Van der Schaft. (2010) A passivity-based approach to reset control systems stability, *Systems & Control Letters*, 59, pp. 18-24.
- [7] J.C. Clegg. (1958) A nonlinear integrator for servomechanisms, *Trans. AIEE*, 77, pp. 41-42.
- [8] B. Hunnekens, N. van de Wouw, M.F. Heertjes, and H. Nijmeijer. (2015) Synthesis of variable gain integral controllers for linear motion systems, *IEEE Trans. on Contr. Syst. Technology*, 23(1), pp. 139-149.
- [9] L. Zaccarian, D. Nešić, and A.R. Teel. (2010) Analytical and numerical Lyapunov functions for SISO linear control systems with first-order reset elements, *Int. J. of Robust & Nonlinear Control*, 21(10), pp. 1134-1158.
- [10] R. Goebel, R.G. Sanfelice, and A.R. Teel. (2012) *Hybrid dynamical systems: modeling, stability and robustness*, Princeton University Press.
- [11] I. Horowitz, P. Rosenbaum. (1975) Non-linear design for cost of feedback reduction in systems with large parameter uncertainty, *Int. J. of Control*, 21(6), pp. 977-1001.